Control and Power Management of Converter Fed Microgrids

Charles K. Sao, *Member, IEEE*, and Peter W. Lehn, *Senior Member, IEEE*

***Abstract*—This paper presents a voltage-power droop/frequency-reactive power boost (VPD/FQB) control scheme that allows multiple voltage source converters (VSCs) to operate in parallel in a VSC fed microgrid. Each current controlled VSC in such a microgrid has its own VPD/FQB controller that sets its current references to regulate the voltage and frequency of a common microgrid bus. By drooping the voltage reference of each controller against its real power output, multiple VPD/FQB controllers jointly regulate the microgrid voltage while sharing a common load power in proportion to a predetermined ratio. Similarly, by boosting the frequency reference of each controller against its reactive power output, multiple VPD/FQB controllers jointly regulate the microgrid frequency while sharing the reactive load in proportion to a predetermined ratio. The proposed control scheme can also operate in grid connected mode. Experimental results are provided to validate the VPD/FQB control scheme.**

***Index Terms*—dq-frame current control, frequency boost, instantaneous synchronization, load sharing, microgrid control, voltage droop, voltage source converter.**

I. Introduction

A SECTION OF the bulk power system with distributed power sources may be called a microgrid if it is capable of operating as a single controllable system [1]. Many new distributed power sources, such as wind turbine generators, microturbines and fuel cells, do not generate 60-Hz ac voltage and therefore require voltage source converters (VSCs) as part of the circuitry to interface them with the microgrid. Thus, a modern microgrid typically includes a network of VSCs that operate in parallel to supply a common load.

It is desirable that a microgrid, which is normally connected to the bulk power system, continue to operate when it becomes islanded. Some important requirements for reliable islanded operation of a VSC fed microgrid are:

1) VSCs must jointly regulate the microgrid bus voltage and frequency;
2) VSCs must share a common load in proportion to a predetermined ratio regardless of plant parameters;
3) VSC control must be achieved using locally measured feedback signals only.

Furthermore, it is desirable to use the same VSC topology and controls in both grid connected and islanded operation and to avoid undesirable interactions between the VSCs and the distribution network [2]. Low voltage ride through (LVRT) is also a requirement for distributed power sources [3].

Manuscript received October 30, 2006; revised December 19, 2007. Paper no. TPWRS-00778-2006.

The authors are with the Department of Electrical and Computer Engineering, University of Toronto, Toronto, ON M5S 3G4 Canada.

Digital Object Identifier 10.1109/TPWRS.2008.922232

The output VSC of a distributed power source has an inductor interface to the grid that is typically regulated by a dq-frame current control. Neither voltage nor the frequency at the point of common coupling (PCC) is normally regulated by the VSC. The frequency of the output current is 60 Hz because the VSC is synchronized to the voltage vector at the PCC. This vector rotates at 60 Hz as dictated by the grid. In contrast, a typical uninterruptible power supply (UPS) VSC operates as a voltage source in islanded mode and employs a frequency generator, such as a crystal oscillator, to set the output frequency to 60 Hz [4]–[6]. Similarly, a frequency generator is used to set the output frequency of the VSC in most published control schemes for islanded VSC fed microgrids [7]–[9]. The VSC also operates as a voltage source.

Reference [10] proposes a supervisory control scheme that allows a single VSC with standard inductor interface and dq frame current control to operate in intentional islanding mode. The scheme, which will be called VP/FQ control scheme in this paper, sets the real power output to regulate the microgrid voltage and the reactive power output to regulate the frequency. However, a VSC with VP/FQ controls cannot operate in parallel with other VSCs on the same islanded microgrid. Neither can it operate in grid connected mode.

This paper proposes the voltage-power droop/frequency-reactive power boost (VPD/FQB) control scheme, which allows current controlled VSCs to operate in parallel on the same microgrid, both in islanded and grid connected modes. Each VSC in the microgrid has its own VPD/FQB controller that sets its current references to regulate the voltage and frequency of a common microgrid bus to track drooped references. Drooping the voltage reference on a VPD/FQB controller of a VSC against its real power output and boosting the frequency reference against its reactive power output enables the VSC to operate in parallel with other VSCs or the bulk power system. This is in stark contrast to the standard generator load sharing scheme [11] and some converter load sharing schemes [1], [7], [12], which droop the source frequency against real power output and voltage against reactive power. In islanded operation, multiple VSCs with VPD/FQB controls jointly regulate the microgrid voltage and frequency and share a common real and reactive load in proportion to their voltage and frequency droop coefficients. In grid connected operation, the microgrid voltage and frequency are dictated by the bulk power system. Each VSC then delivers real and reactive power as determined by the voltage and frequency references and the droop coefficients of its VPD/FQB controller.

II. Multi-VSC-Fed Microgrid

A simplified microgrid with multiple VSCs is shown in Fig. 1. The microgrid consists of a collector bus, a bus capacitor, C_B,

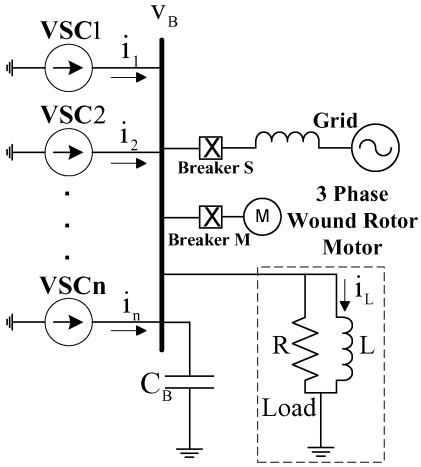

Fig. 1. Microgrid fed by VSC1 and VSC2.

a motor load and a static load, which is represented as a parallel combination of resistance R and inductance L. The motor is a three phase, wound rotor machine. It is assumed that the load is balanced and that the line impedance between the collector bus and the load is small. The microgrid may be connected to the bulk power system through circuit breaker S. The VSCs employ high bandwidth current controllers, consequently, the VSCs together with their interface inductors are modelled as current sources. Converter currents are assumed equal to their current controller reference values. The model is an extension of the single VSC fed microgrid of [10].

The dynamic model of the microgrid of Fig. 1 is formulated in reference frame U, which is instantaneously synchronized to the capacitor voltage vector $\vec{v}_B$. The large signal equations of the model are

$$\begin{aligned}\frac{dv_{Bd}}{dt} &= -\frac{v_{Bd}}{RC_B} - \frac{i_{Ld}}{C_B} + \frac{\sum_{k=1}^{k=n} i_{kd}}{C_B}\\ \frac{di_{Ld}}{dt} &= \frac{v_{Bd}}{L} + \frac{\sum_{k=1}^{k=n} i_{kq} - i_{Lq}}{C_B v_{Bd}} i_{Lq}\\ \frac{di_{Lq}}{dt} &= -\frac{\sum_{k=1}^{k=n} i_{kq} - i_{Lq}}{C_B v_{Bd}} i_{Ld}\end{aligned} \tag{1}$$

where

v_{Bd}	d-axis components of $\vec{v}_B^{(U)}$;
i_{Ld} and i_{Lq}	d and q axis components of $\vec{i}_L^{(U)}$;
i_{kd} and i_{kq}	d and q axis components of $\vec{i}_k^{(U)}$, the current vector of VSC number k in reference frame U.

The magnitude, v_B, and instantaneous frequency, ω_B, of the collector bus voltage vector, $\vec{v}_B$, are the outputs to be regulated. They are given in terms of the state variables v_{Bd}, i_{Ld} and i_{Lq}, and inputs i_{kd} and i_{kq} by

$$v_B = v_{Bd} \tag{2}$$

$$\omega_B = \frac{\sum_{k=1}^{k=n} i_{kq} - i_{Lq}}{C_B v_{Bd}}. \tag{3}$$

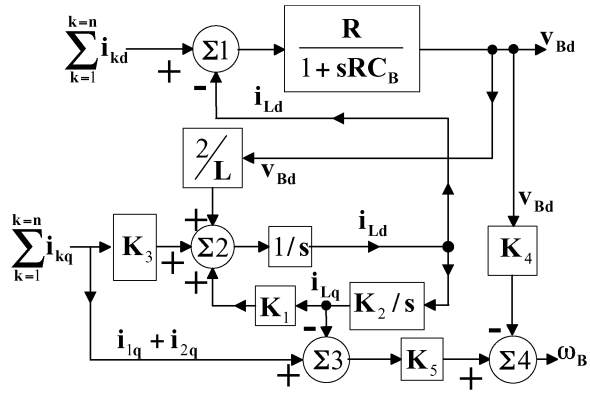

Fig. 2. Block diagram representation of the linearized model of the microgrid in Fig. 1 (motor excluded).

It can be shown that only one feasible operating point of the nonlinear state space model exists. The operating point is

$$v_{Bd0} = R\sum_{k=1}^{k=n} i_{kd0} \tag{4}$$

$$i_{Ld0} = 0 \tag{5}$$

$$i_{Lq0} = \frac{\sum_{k=1}^{k=n} i_{kq0}}{2} - \sqrt{\left(\frac{\sum_{k=1}^{k=n} i_{kq0}}{2}\right)^2 + \frac{C_B\left(R\sum_{k=1}^{k=n} i_{kd0}\right)^2}{L}}. \tag{6}$$

The corresponding steady state outputs are

$$v_{B0} = v_{Bd0} = R\sum_{k=1}^{k=n} i_{kd0} \tag{7}$$

$$\omega_{B0} = \frac{\sum_{k=1}^{k=n} i_{kq0}}{2RC_B\sum_{k=1}^{k=n} i_{kd0}} + \sqrt{\left(\frac{\sum_{k=1}^{k=n} i_{kq0}}{2C_B R\sum_{k=1}^{k=n} i_{kd0}}\right)^2 + \frac{1}{LC_B}}. \tag{8}$$

A linearized model of the microgrid about this operating point is shown in Fig. 2, where

$$K_1 = \frac{\sum_{k=1}^{k=n} i_{kq0} - 2i_{Lq0}}{Cv_{Bd0}} \quad K_2 = \frac{i_{Lq0} - \sum_{k=1}^{k=n} i_{kq0}}{Cv_{Bd0}}$$

$$K_3 = \frac{i_{Lq0}}{Cv_{Bd0}} \quad K_4 = \frac{\sum_{k=1}^{k=n} i_{kq0} - i_{Lq0}}{Cv_{Bd0}^2} \quad K_5 = \frac{1}{Cv_{Bd0}}.$$

Equation (7) shows that only d-axis VSC currents influence v_{B0}. Thus d-axis current must be controlled to regulate bus voltage.

In contrast, (8) shows that ω_{B0} is a non-linear function of Σi_{d0} and Σi_{q0}. Since Σi_{d0} is employed for voltage control, only Σi_{q0} is available for frequency control.

III. Review of VP/FQ Control Scheme

The VP/FQ control scheme, presented in [10], has been developed for a microgrid fed by a single VSC. The control design is based on the linearized microgrid model shown in Fig. 2, for

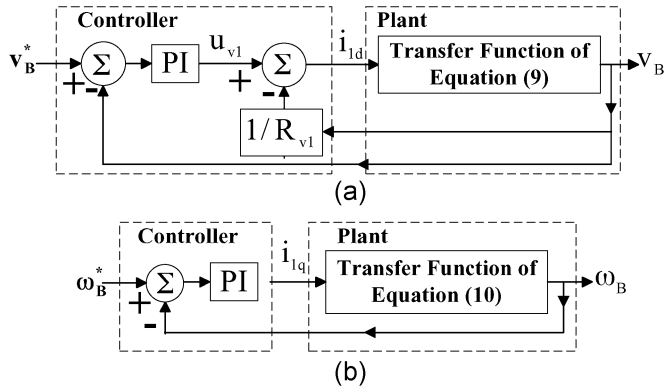

Fig. 3. Voltage and frequency loops of the VP/FQ control scheme [10].

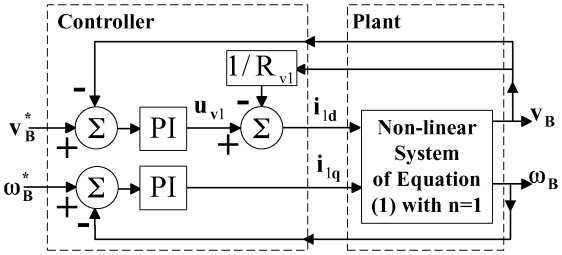

Fig. 4. Large signal representation of the VP/FQ control scheme [10].

the case $n = 1$. The VP/FQ control consists of voltage and frequency control loops to regulate bus voltage, v_B, and frequency, ω_B.

A voltage control loop is designed based on the nominal transfer function relating d-axis VSC current to the microgrid bus voltage

$$\frac{v_B(s)}{i_{1d}(s)} = \frac{\frac{1}{C_B}s^2 - \frac{K_1K_2}{C_B}}{s^3 + \frac{1}{RC_B}s^2 + \left(\frac{2}{LC_B} - K_1K_2\right)s - \frac{K_1K_2}{RC_B}}. \quad (9)$$

The voltage control loop, which is shown in Fig. 3(a), employs a PI compensator to regulate v_B to the voltage reference v_B^*. It is demonstrated in [10] that the resulting system is robust under all loading conditions.

A frequency control loop, shown in Fig. 3(b), is designed based on the transfer function relating q-axis VSC current to the microgrid bus frequency, given by (10) at the bottom of the page. Due to cross-coupling, dynamics of the inner voltage control loop must be included in this transfer function to ensure overall system stability [10]. A block diagram representation of the entire closed loop system is shown in Fig. 4.

TABLE I
VSC RATING AND CONTROL PARAMETERS

Parameters and Variables	Values
VSC Rated Voltage	V_{Rated} = 94 V_{LN} (Pk), 115 V_{LL} (rms)
VSC Rated Current	I_{Rated} = 35.5 A (Pk), 25 A (rms)
v_B Control Proportional Gain	K_{pv1} = 0.45
v_B Control Integral Gain	K_{iv1} = 58.5
Virtual Resistance	R_{v1} = 7.94 Ω 3 $p.u.$
ω_B Control Proportional Gain	$K_{p\omega 1}$ = 0.035
ω_B Control Integral Gain	$K_{i\omega 1}$ = 24.5

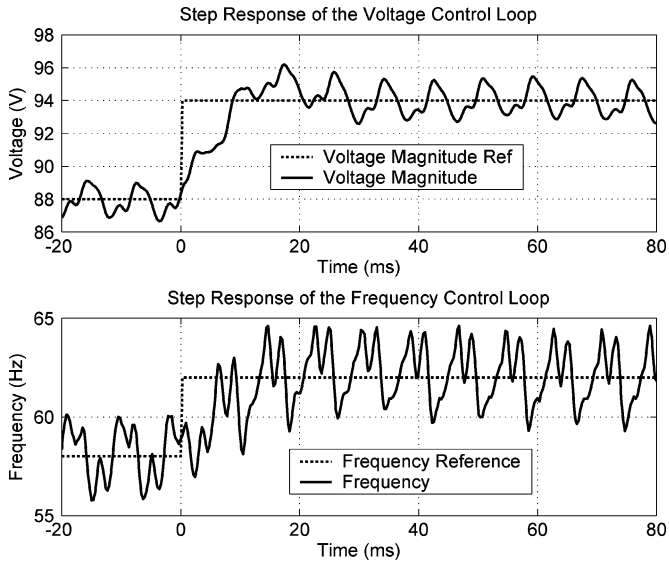

Fig. 5. Experimentally obtained step response of the voltage and frequency loops of the VP/FQ control scheme.

The VP/FQ control scheme has been experimentally validated under the worst-case condition of infinite load resistance R (i.e., minimal system damping). The capacitance C_B is 300 μF and the load inductance is $L = 16.5$ mH. Controller parameters are listed in Table I. Fig. 5 shows the response of the voltage control loop to a step change in v_B^* from 88 to 94 V,

$$\frac{\omega_B(s)}{i_{1q}(s)} = \frac{s^4 + A_3s^3 + A_2s^2 - A_1s - \frac{K_{iv}}{C_B}(K_{12} + K_{23})}{C_B v_{Bd0}\left(s^4 + \left(\frac{1}{R_{e1}C_B} + \frac{K_{pv}}{C_B}\right)s^3 + \left(\frac{2}{LC_B} - K_{12} + \frac{K_{iv}}{C_B}\right)s^2 - \left(\frac{K_{12}}{R_{e1}C_B} + \frac{K_{12}K_{pv}}{C_B}\right)s - \frac{K_{12}K_{iv}}{C_B}\right)}$$

$$\text{where } A_3 = \left(\frac{1}{R_{e1}C_B} + \frac{K_{pv}}{C_B}\right)$$

$$A_2 = \left(\frac{2}{LC_B} - K_{12} + \frac{K_{iv}}{C_B} - K_{23} + K_{34}v_{Bd0}\right)$$

$$A_1 = \left(\frac{K_{12}}{R_{e1}C_B} + \frac{K_{12}K_{pv}}{C_B} + \frac{K_{23}}{R_{e1}C_B} + \frac{K_{23}K_{pv}}{C_B}\right)$$

$$K_{12} = K_1K_2 \qquad K_{23} = K_2K_3 \qquad K_{34} = K_3K_4 \quad (10)$$

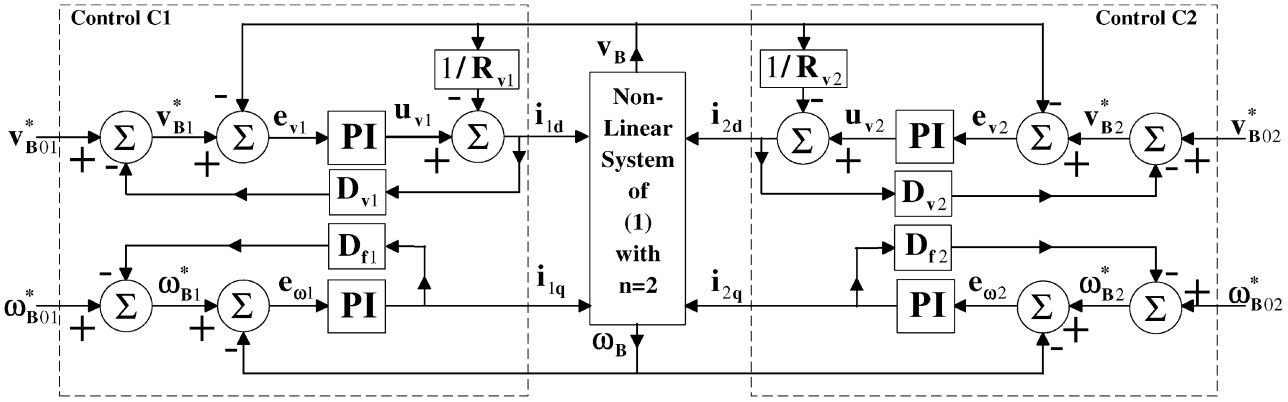

Fig. 6. Proposed VPD/FQB controllers for the microgrid in Fig. 1.

and the response of the frequency control loop to a step change in ω_B^* from 58 to 62 Hz. Even though the plant contains no resistive damping component, voltage and frequency responses are well damped and settle in about one cycle.

IV. VPD/FQB Control Scheme

The VPD/FQB control scheme is proposed for multi-VSC-fed microgrids. To simplify analysis, a microgrid with only two VSCs will be analyzed $(n = 2)$. Each VSC has its own VPD/FQB controller. These VPD/FQB controllers operate in parallel to jointly regulate the voltage and frequency of the microgrid as shown in Fig. 6. Based on the observation that only inputs i_{1d} and i_{2d} influence v_{Bd} and that i_{1q} and i_{2q} are the remaining inputs available for regulating ω_B, these VPD/FQB controllers set i_{1d} and i_{2d} to regulate v_B and set i_{1q} and i_{2q} to regulate ω_B.

Similar to parallel operating generators that cannot use speed governors with fixed speed references [11], the VPD/FQB controllers cannot use fixed references to regulate the microgrid voltage and frequency. An analysis of the droop characteristic of two parallel operating generators is presented to justify the drooped voltage and frequency references of the VPD/FQB controllers.

A. Analysis of Generator Speed Droop Scheme

Two turbine generator units and their speed governors are shown in Fig. 7. These generators supply an isolated power system with a single main bus. Governor G1 regulates N_1, the shaft speed of turbine T1, to track N_1^*, which is drooped against Y_1, the position of the water/steam intake gate/valve of T1 [11]. Governor G2 regulates N_2 in a similar manner. Assuming stability, the steady state solution for speeds N_1 and N_2 of turbine generator units 1 and 2 are

$$N_1 = N_{01}^* - D_1 Y_1 \tag{11}$$
$$N_2 = N_{02}^* - D_2 Y_2 \tag{12}$$

where N_{01} and D_1 are the no-load speed reference and speed droop coefficient of governor G1.

N_{02} and D_2 are the no-load speed reference and speed droop coefficient of governor G2.

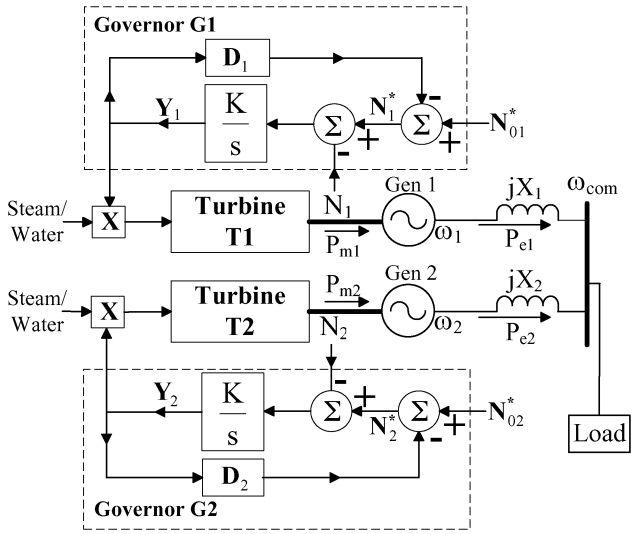

Fig. 7. Two generators and their speed governors with droop characteristics.

If the two generators have the same number of poles, p, their steady state electrical frequencies are given by

$$\omega_1 = \frac{p}{2}\left(N_{01}^* - D_1 Y_1\right) \tag{13}$$
$$\omega_2 = \frac{p}{2}\left(N_{02}^* - D_2 Y_2\right). \tag{14}$$

Under steady state conditions the system frequency ω_{com} is equal to both ω_1 and ω_2, and given by

$$\omega_{com} = \frac{p}{2}\left(N_{01}^* - D_1 Y_1\right) = \frac{p}{2}\left(N_{01}^* - D_1 Y_1\right). \tag{15}$$

Speed governors G1 and G2 jointly, albeit indirectly, regulate ω_{com} by tracking reference speeds that are drooped against Y_1 and Y_2, respectively. If no-load speed references N_{01}^* and N_{02}^* are identical, the steady state gate/valve positions of the two turbines obey the equation

$$Y_1 : Y_2 = D_2 : D_1. \tag{16}$$

The relationship between the gate/valve position of a turbine and its output mechanical power is assumed to be linear in a

typical analysis of generator speed governors [11]. Thus, the ratio of mechanical turbine output powers P_{m1} to P_{m2} is

$$P_{m1} : P_{m2} = D_2 : D_1. \tag{17}$$

Neglecting generator losses, (17) shows that the two turbine generator units share the electrical load in proportion to the droop coefficients D_2 and D_1.

In summary, the speed governors of T1 and T2 are able to regulate ω_{com} (a common output) jointly, albeit indirectly, without fighting with one another because they employ variable speed references that are drooped against Y_1 and Y_2 (control inputs). These drooped references allow the two turbine generators to share a common load in proportion to a predetermined ratio.

B. Drooped References of the VPD/FQB Control

Based on the observations of Section IV-A, the VPD/FQB controllers in Fig. 6 are synthesized such that:

1) they employ voltage references v^*_{B1} and v^*_{B2} that are drooped against control inputs i_{1d} and i_{2d}, respectively, to jointly regulate v_B (a common output) and to share a common real load on the microgrid in proportion to the voltage droop coefficients D_{v2} and D_{v1};
2) they employ frequency references ω^*_{B1} and ω^*_{B2} that are drooped against control inputs i_{1q} and i_{2q}, respectively, to jointly regulate ω_B (a common output) and to share a common reactive load on the microgrid in proportion to the frequency droop coefficients $D_{\omega 2}$ and $D_{\omega 1}$. (Drooping ω^*_{B1} and ω^*_{B2} against i_{1q} and i_{2q} is equivalent to boosting these references against Q_1 and Q_2 because $Q_1 = -1.5 v_B i_{1q}$ and $Q_2 = -1.5 v_B i_{2q}$.)

C. Joint Voltage Control and Real Power Sharing

The voltage loop of controller C1 sets the d-axis current of VSC1 as shown in Fig. 6. A PI compensator regulates the bus voltage to track v^*_{B1}, a voltage reference that is drooped against i_{1d} as per (18). The controller includes a virtual resistance to ensure that the PI compensator sees a stable plant regardless of the resistive load (R) on the microgrid [10].

Since v^*_{B1} is equal to v^*_{B01} when there is no resistive load on the microgrid, v^*_{B01} is referred to as the no-load voltage reference. The control laws of the voltage loop may be expressed mathematically as

$$v^*_{B1} = v^*_{B01} - D_{v1} i_{1d} \tag{18}$$

$$u_{v1} = \left(K_{pv1} + \frac{K_{iv1}}{s}\right)(v^*_{B1} - v_B) \tag{19}$$

$$i_{1d} = u_{v1} - \frac{v_B}{R_{v1}} \tag{20}$$

where K_{pv1} and K_{iv1} are the proportional and integral gains of the voltage loop PI compensator of controller C1; D_{v1} is the voltage droop coefficient of controller C1.

Assuming stability, the input to the PI compensator of (19) is zero when the closed loop system reaches steady state. Thus, in steady state

$$v_B = v^*_{B1} = v^*_{B01} - D_{v1} i_{1d}. \tag{21}$$

Similarly, the voltage loop of controller C2 yields

$$v_B = v^*_{B2} = v^*_{B02} - D_{v2} i_{2d}. \tag{22}$$

Since (21) and (22) are simultaneously satisfied, an implicit relation exists between the d-axis currents of the two VSCs. Provided that the no-load voltage references v^*_{B01} and v^*_{B02} are identical, the steady state d-axis currents of the VSCs satisfy

$$\frac{i_{1d}}{i_{2d}} = \frac{D_{v2}}{D_{v1}}. \tag{23}$$

Furthermore, the q-axis collector bus voltage (v_{Bq}) is always zero, and the real powers delivered by VSC1 and VSC2 are $P_1 = 1.5 v_B i_{1d}$ and $P_2 = 1.5 v_B i_{2d}$, respectively. Thus, the voltage droop coefficients determine the distribution of the real load between the two VSCs according to

$$\frac{P_1}{P_2} = \frac{D_{v2}}{D_{v1}}. \tag{24}$$

Equation (24) shows that steady real power allocation between the two VSCs is determined solely by their voltage droop coefficients. Microgrid parameters do not influence the steady state real power sharing among the VSCs.

D. Joint Frequency Control and Reactive Power Sharing

The frequency loop of controller C1 sets the q-axis current of VSC1, as shown in Fig. 6. A PI compensator regulates the bus frequency to track ω^*_{B1}, a frequency reference that is drooped against i_{1q} as per (25).

Since ω^*_{B1} is equal to ω^*_{B01} when the VSC does not supply any reactive power to the microgrid, ω^*_{B01} is referred to as the no-load frequency reference. The control laws of the frequency loop may be expressed mathematically as

$$\omega^*_{B1} = \omega^*_{B01} - D_{\omega 1} i_{1q} \tag{25}$$

$$i_{1q} = \left(K_{p\omega 1} + \frac{K_{i\omega 1}}{s}\right)(\omega^*_{B1} - \omega_B) \tag{26}$$

where $K_{p\omega 1}$ and $K_{i\omega 1}$ are the proportional and integral gains of the frequency loop PI compensator; $D_{\omega 1}$ is the frequency droop coefficient.

Assuming stability, the input to the PI compensator is zero when the closed loop system reaches steady state. Thus, in steady state

$$\omega_B = \omega^*_{B2} = \omega^*_{B01} - D_{\omega 1} i_{1q}. \tag{27}$$

Similarly, the frequency loop of controller C2 yields

$$\omega_B = \omega^*_{B2} = \omega^*_{B02} - D_{\omega 2} i_{2q}. \tag{28}$$

Since (27) and (28) are simultaneously satisfied, an implicit relation exists between the q-axis currents of the two VSCs. Provided that the no-load frequency references ω^*_{B01} and ω^*_{B02} are identical, the steady state q-axis currents of the VSCs satisfy

$$\frac{i_{1q}}{i_{2q}} = \frac{D_{\omega 2}}{D_{\omega 1}}. \tag{29}$$

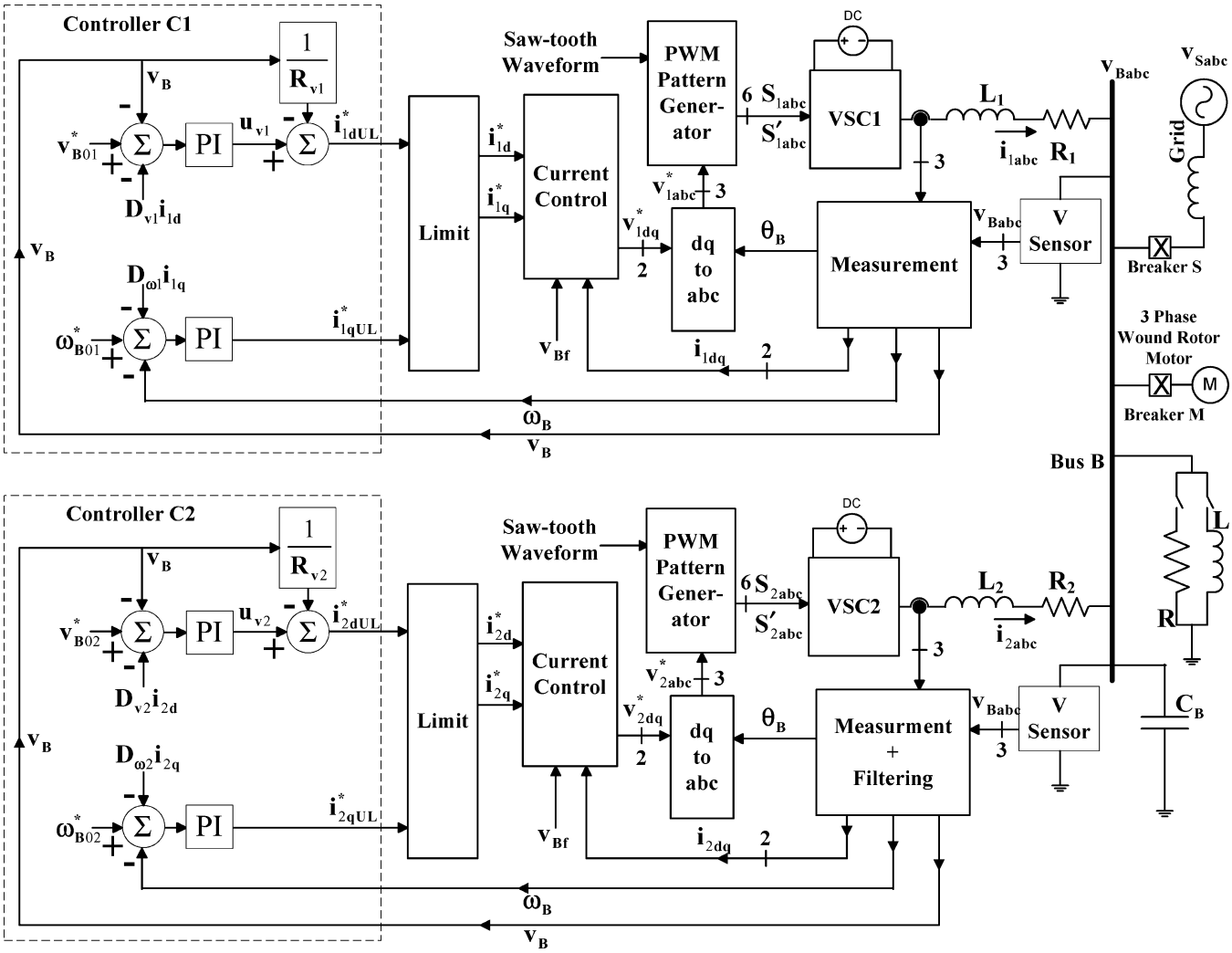

Fig. 8. Experimental microgrid and its controls.

The reactive powers delivered by VSC1 and VSC2 are $Q_1 = -1.5v_B i_{1q}$ and $Q_2 = -1.5v_B i_{2q}$, respectively. Thus, the frequency droop coefficients determine the distribution of the reactive load between the two VSCs according to

$$\frac{Q_1}{Q_2} = \frac{D_{\omega 2}}{D_{\omega 1}}. \tag{30}$$

Equation (30) shows that steady reactive power allocation between the two VSCs is determined solely by their frequency droop coefficients. Microgrid parameters do not influence the steady state reactive power sharing among the VSCs.

TABLE II
MICROGRID PARAMETERS

Parameters	Values
Base Voltage	V_{Base} = 94 V_{LN} (Pk) 115 V_{LL} (rms)
Base Current	I_{Base} = 35.5 A (Pk) 25 A (rms)
Base Impedance	Z_{Base} = 2.65 Ω
Microgrid Rated Voltage	V_{Rated} = 94 V_{LN} (Pk) (1 $p.u.$)
Rated Current of VSCs	I_{Rated} = 35.5 A (Pk) (1 $p.u.$)
Microgrid Bus Capacitance	C_B = 304.5 μF (0.3 $p.u.$)
Load Resistance	R = 3.9 Ω (1.47 $p.u.$)
Load Inductance	L = 16.5 mH (2.35 $p.u.$)
VSC1 Interface L	L_1 = 0.65 mH (0.092 $p.u.$)
VSC1 Conduction Loss	R_1 = 171 $m\Omega$ (0.065 $p.u.$)
VSC2 Interface L	L_2 = 1.16 mH (0.166 $p.u.$)
VSC2 Conduction Loss	R_2 = 165 $m\Omega$ (0.062 $p.u.$)

V. EXPERIMENTAL RESULTS—ISLANDED OPERATION

A simplified microgrid is set up in the laboratory to validate the control scheme of Section IV. The schematic diagram of the microgrid and its controls are shown in Fig. 8. The ratings and parameters of the microgrid are listed in Table II. Note that resistances R_1 and R_2 represent conduction losses of the converters and their interface inductors.

A. Validating the VPD/FQB Control Scheme With Static Load

This experiment validates joint microgrid control and load sharing of controllers C1 and C2 by activating C2 while VSC1 (with controller C1) is feeding the islanded microgrid as its sole power source. Table III lists the parameters of C1. C2 is identical to C1. Prior to activating C2:

1) both VSC1 and VSC2 are connected to the microgrid;

TABLE III
PARAMETERS OF CONTROLLER C1

Parameters	Values
C1 No-load Voltage Reference	v^*_{B01} = 94 V
C1 Voltage Droop Coefficient	D_{v1} = 0.1 V/A1
C1 v_B Control Proportional Gain	K_{pv1} = 0.45
C1 v_B Control Integral Gain	K_{iv1} = 58.5
C1 Virtual Resistance	R_{v1} = 7.94 Ω (3 $p.u.$)
C1 No-load Frequency Reference	ω^*_{B01} = 376.991 rad/s
C1 Frequency Droop Coefficient	$D_{\omega 1}$ = 0.2 $rad/s/A$
C1 ω_B Control Proportional Gain	$K_{p\omega 1}$ = 0.035
C1 ω_B Control Integral Gain	$K_{i\omega 1}$ = 24.5

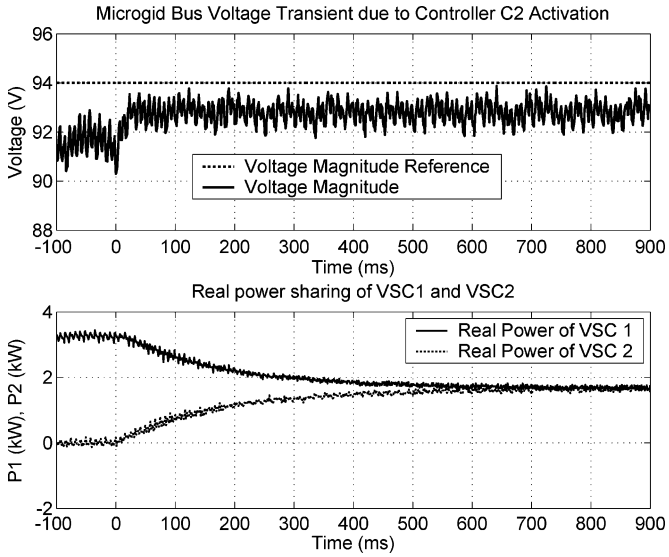

Fig. 9. Joint regulation of v_B by VSC1 and VSC2 and sharing of a common real load upon activating controller C2.

2) the dq frame current references of VSC2 are held at zero, leaving VSC1 to supply the entire load;
3) the resistive load is $R = 3.9\ \Omega$ (1.47 p.u.). The inductive load (L) and the motor are switched out.

Fig. 9 demonstrates joint control of v_B and real power sharing by VPD/FQB controllers C1 and C2. Initially, P_1 is 3.26 kW and the microgrid voltage is $v_B = 91.6$ V. When controller C2 is activated at $t = 0$ ms, the real power output of VSC2 increases until both VSCs output 1.67 kW each. The d-axis currents of the VSCs are $i_{1d} = i_{2d} = 12$ A. Thus, the theoretical steady state microgrid voltage is $v_B = (94 - 0.1 * 12) = 92.8$ V. Fig. 9 shows that v_B settles to approximately 93 V.

Fig. 10 demonstrates joint control of ω_B and reactive power sharing by VPD/FQB controllers C1 and C2. Initially, VSC1 is absorbing 1.44 kVAR from the bus capacitor (C_B) and the microgrid frequency is 59.67 Hz. When controller C2 is activated at $t = 0$ ms, the reactive power output of VSC2 decreases until both VSCs output -0.74 kVAr. The q-axis currents of the VSCs are $i_{1q} = i_{2q} = 5.31$ A. Thus, the theoretical steady state microgrid frequency is $\omega_B = \omega^*_{B1} = (376.9911 - 0.2 * 5.31) = 375.94$ rad/s or 59.83 Hz. Fig. 10 shows that ω_B settles to approximately 59.8 Hz.

Note that the load draws higher real and reactive power after activating C2 because the steady state voltage rises from 91.6 V to approximately 92.8 V as a result of activating C2.

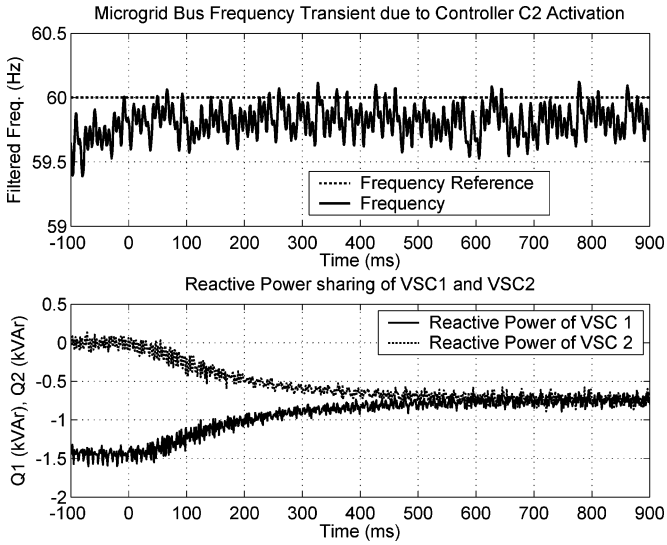

Fig. 10. Joint regulation of ω_B by VSC1 and VSC2 and sharing of a common reactive load upon activating controller C2.

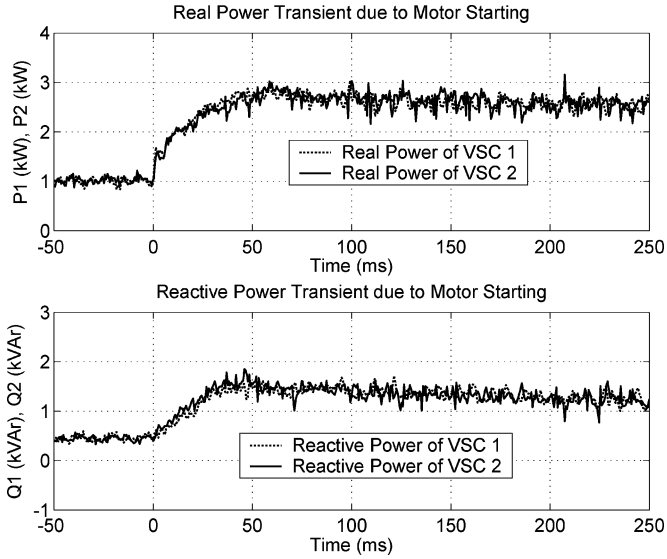

Fig. 11. Real and reactive power output transient of VSC1 and VSC2 due to motor starting.

B. Validating the VPD/FQB Control Scheme With Motor Load

To test the robustness of the VPD/FQB control scheme, this experiment starts up the motor in Fig. 1 while the VSCs are supplying the islanded microgrid. The rated speed and power of the motor are 3420 rpm and 1 hp. Table III lists the parameters of identical controllers C1 and C2. Prior to starting the motor:

1) the resistive load is $R = 6.3\ \Omega$ (2.37 p.u.). The inductive load (L) is switched out;
2) Breaker M (see Fig. 1) is closed and the motor is energized, but its rotor is open circuited. The motor shaft is coupled to a mechanical load whose torque is proportional to the motor speed.

Figs. 11 and 12 show the experiment response of the VPD/FQB controllers to motor start-up. Prior to starting the motor, $P_1 = P_2 = 1$ kW and $Q_1 = Q_2 = -0.6$ kVAr. Moreover, $v_B = 93.3$ V and $\omega_B = 377.65$ rad/s or 60.1 Hz.

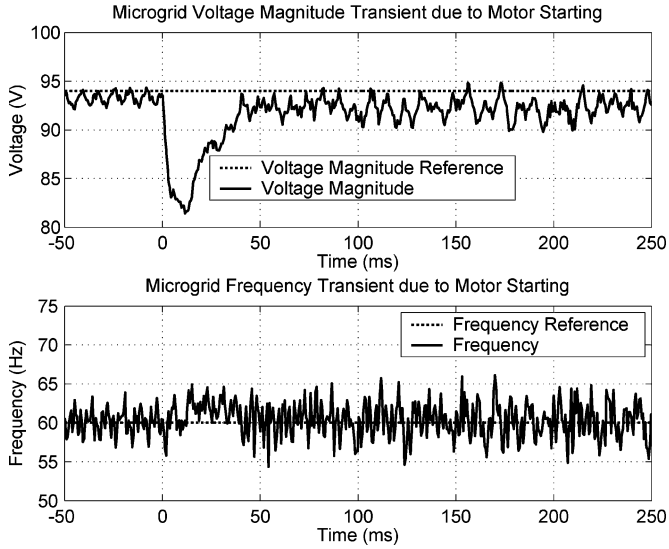

Fig. 12. v_B and ω_B transient due to motor starting.

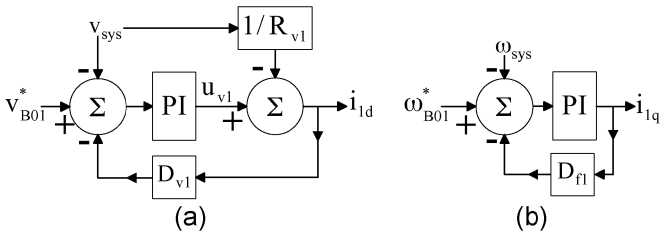

Fig. 13. Voltage and frequency control loops of VPD/FQB controller C1 in grid connected operation.

The loaded motor is started by closing the three phases of the rotor circuit through 1.5 Ω resistors. *In response to the increased load, the power outputs of VSC1 and VSC2 increase simultaneously as shown in* Fig. 11. *Power is shared equally throughout the transient, avoiding transient over current in any one VSC.* During the motor starting transient the microgrid voltage (v_B) drops to 81 V and recovers within approximately two cycles as shown in Fig. 12. It can be seen that the frequency also fluctuates during the transient and settles down within two cycles. As of $t = 250$ ms, the motor has not yet reached a mechanical steady state operating point, though the electrical quantities have reached a quasi steady state. The 1-hp motor is still drawing approximately 1.5 kW from each VSC.

VI. Grid Connected Operation

This section describes the behavior of the VPD/FQB control scheme when the microgrid is in grid connected operation. It is assumed that the fault MVA of the bulk power system at the PCC with the microgrid bus is much larger than the MVA ratings of the VSCs. Thus, v_B and ω_B are no longer significantly influenced by the VSC currents. Instead, they are set by the bulk power system. Thus, $v_B = v_{sys}$ and $\omega_B = \omega_{sys}$ where v_{sys} and ω_{sys} are the voltage and frequency of the bulk power system at the PCC with the microgrid. Holding v_B and ω_B constant decouples the voltage and frequency control loops of controller C1 as shown in Fig. 13.

With v_B set by the grid, the only state variable in the voltage loop of controller C1 is i_{1d}. In s-domain, $i_{1d}(s)$ is expressed in terms of no-load voltage reference (v^*_{B01}) and the grid voltage (v_{sys}) as per (31). Its steady state solution is given by

$$i_{1d}(s) = \frac{(K_{pv1}s + K_{iv1})\,(v^*_{B01}(s) - v_{sys}(s))}{(1 + K_{pv1}D_{v1})s + K_{iv1}D_{v1}} \tag{31}$$

$$i_{1d} = \frac{(v^*_{B01} - v_{sys})}{D_{v1}}. \tag{32}$$

It also follows from (31) that the closed loop eigenvalue λ_{v1} and time constant τ_{v1} of the voltage loop of C1 in grid connected operation is

$$\lambda_{v1} = \frac{1}{\tau_{v1}} = -\frac{K_{iv1}D_{v1}}{1 + K_{pv1}D_{v1}}. \tag{33}$$

Equations (31) –(33) imply that:

1) setting v_B constant turns the voltage loop into a first order system with input v^*_{B01} and output i_{1d};
2) the no-load voltage reference (v^*_{B01}) may be used to regulate i_{1d}, and hence the real power output, of VSC1 in grid connected mode;
3) the voltage loop of the VPD/FQB controller is large signal stable in the grid connected mode if K_{pv1}, K_{iv1} and D_{v1} are positive numbers and the underlying current control loop is stable;
4) the closed loop bandwidth of the voltage loop depends on the product of K_{iv1} and D_{v1} if $(K_{pv1}D_{v1}) \ll 1$. Thus, the dynamics of real power control in grid connected operation can be tuned without affecting voltage regulation in the islanded mode.

Similarly, i_{1q} is the only state variable in the frequency control loop when ω_B is set by the grid. $i_{1q}(s)$ is expressed in terms of no-load frequency reference (ω^*_{B01}) and the grid frequency (ω_{sys}) as per (34). Its steady state solution is given by

$$i_{1q}(s) = \frac{(K_{p\omega1}s + K_{i\omega1})\,(\omega^*_{B01}(s) - \omega_B(s))}{(1 + K_{p\omega1}D_{\omega1})s + K_{i\omega1}D_{\omega1}} \tag{34}$$

$$i_{1q} = \frac{(\omega^*_{B01} - \omega_{sys})}{D_{\omega1}}. \tag{35}$$

Again, from (34), the closed loop eigenvalue $\lambda_{\omega1}$ and time constant $\tau_{\omega1}$ of the frequency loop of C1 in grid connected operation is

$$\lambda_{\omega1} = \frac{1}{\tau_{\omega1}} = -\frac{K_{i\omega1}D_{\omega1}}{1 + K_{p\omega1}D_{\omega1}}. \tag{36}$$

Equations (34)–(36) imply that:

1) setting ω_B constant turns the frequency loop into a first order system with input ω^*_{B01} and output i_{1q};
2) the no-load frequency reference (ω^*_{B01}) may be used to regulate i_{1q}, and hence the reactive power output, of VSC1 in grid connected mode;
3) the frequency loop of a VPD/FQB controller is large signal stable in the grid connected mode if $K_{p\omega1}$, $K_{i\omega1}$ and $D_{\omega1}$ are positive numbers and the underlying current control loop is stable;
4) the closed loop bandwidth of the frequency loop depends on the product of $K_{i\omega1}$ and $D_{\omega1}$ if $(K_{p\omega1}D_{\omega1}) \ll 1$. Thus, the dynamics of reactive power control in grid connected

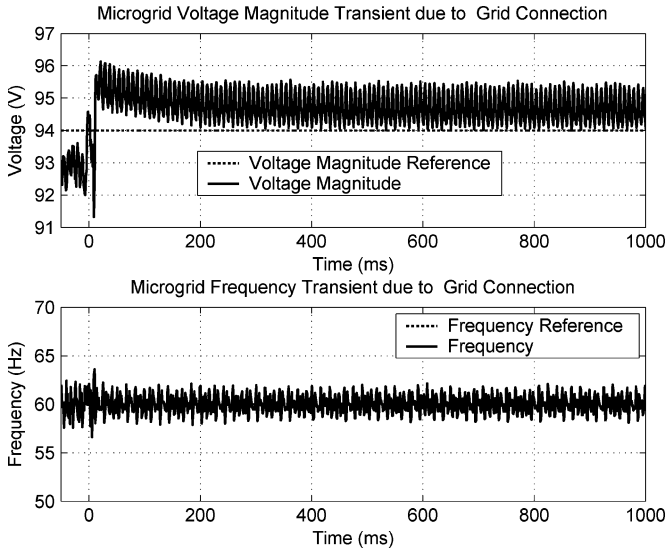

Fig. 14. v_B and ω_B transient due to grid connection.

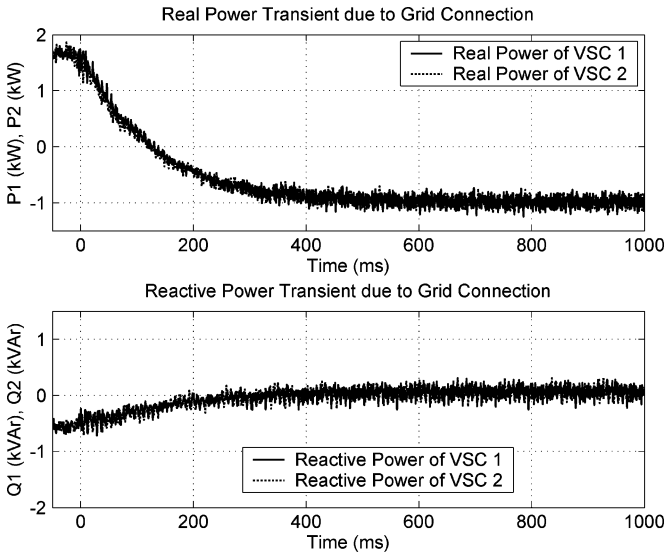

Fig. 15. Real and reactive power output transient of VSC1 and VSC2 due to grid connection.

mode can be tuned without affecting frequency regulation in the islanded mode.

Analogous relations may be found for controller C2.

VII. Experimental Results—Grid Connection and Islanding

The simplified microgrid of Fig. 8 is used to conduct the following experiments. The ratings and parameters of the microgrid are listed in Table II.

A. Grid Connection Test

In this experiment, the microgrid bus is connected to the bulk power system by closing breaker S in Fig. 1 when the microgrid voltage is in phase with the ac supply voltage. Table III lists the parameters of identical controllers C1 and C2. Prior to grid connection, the resistive and inductive loads are $R = 3.9\ \Omega$ (1.47 p.u.) and $L = 99.4\ \mathrm{mH}$ (14.2 p.u.). The motor is switched out.

The bus voltage and frequency transients due to grid connection are shown in Fig. 14 whereas the real and reactive power output transients of the VSCs are plotted in Fig. 15. Initially, each VSC is delivering 1.76 kW and -0.74 kVAR to the microgrid. The microgrid voltage and frequency are $v_B = 92.74$ V and $\omega_B = 375.94\ \mathrm{rad/s}$ or 59.83 Hz.

The voltage and frequency of the bulk power system at the PCC with the microgrid are 95.5 V and 60 Hz previous to closing breaker S. In response to grid connection at $t = 0\ \mathrm{ms}$, v_B and ω_B immediately adjust to 95.5 V and 60 Hz as shown in Fig. 14. Due to the limited strength of the bulk power system, v_B gradually drops to 94.7 V as the microgrid starts drawing power from the ac supply. For the given values of v_{01}^* and v_{02}^*, and a steady state bus voltage of $v_B = 94.7$ V, the theoretical steady state real power outputs of the VSCs are $P_1 = P_2 = 1.5 * 94.7 * (94 - 94.7)/0.1 = -995$ W. It can be seen from the top graph of Fig. 15 that the real power outputs of the VSCs settle down at approximately -1 kW. Thus the experimental results are in agreement with the theoretical prediction. Since ω_{01}^* and ω_{02}^* are both set to 377 rad/s, the steady state values of Q_1 and Q_2 in grid connected operation are expected to be around 0 kVAR. It can be seen from the bottom graph of Fig. 15 that the reactive power outputs of the VSCs settle down at approximately 0 kVAr. Once again, the experimental results are in agreement with the theoretical prediction.

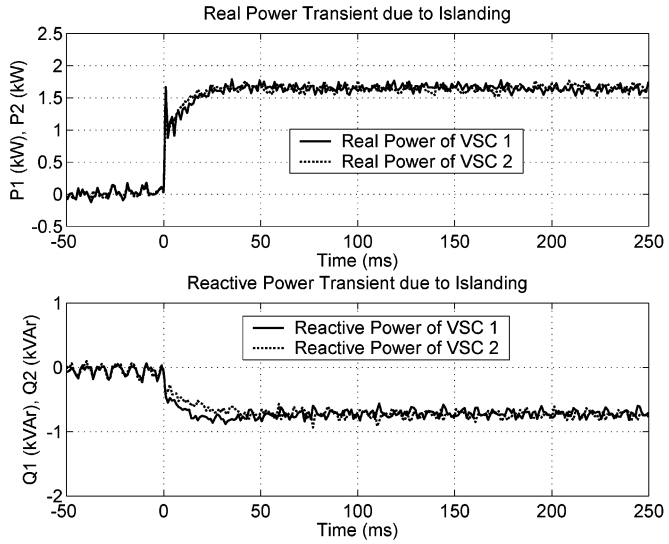

Fig. 16. Real and reactive power output transient of VSC1 and VSC2 due to islanding.

B. Islanding Test

To ascertain that the VPD/FQB control scheme is robust to islanding transients, the microgrid is islanded under relatively heavy load by tripping circuit breaker S in Fig. 1. Table III lists the parameters of identical controllers C1 and C2. Both VSC1 and VSC2 are connected to the microgrid prior to islanding but supplying nearly none of the load. Before islanding occurs, the resistive load is $R = 3.9\ \Omega$ (1.47 p.u.). The inductive load (L) and the motor are switched out.

Fig. 16 shows the real and reactive power outputs of the VSCs. Prior to islanding, the grid supplies almost the entire microgrid load. Upon islanding, the VSCs have to immediately

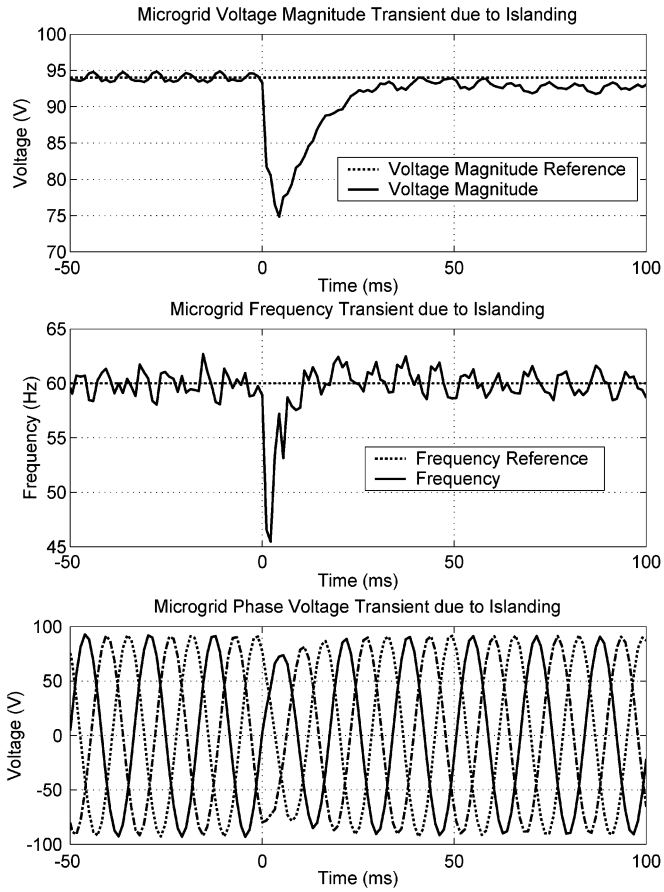

Fig. 17. v_B, ω_B, and v_{Babc} transient due to islanding.

supply the entire resistive load and absorb all the reactive power from the capacitor. As a result, the real power output of each VSC increases to 1.67 kW while the reactive power output decreases to -0.74 kVAr within 40 ms.

The voltage and frequency transients due to islanding are shown in the first two graphs of Fig. 17. The bus voltage (v_B) decreases from 94 V (1.0 p.u.) to 75 V (0.79 p.u.) due to islanding and then recovers to 92 V (0.97 p.u.) within two cycles and settles to 92.8 V. The microgrid frequency (ω_B) also drops from 60 Hz to 43 Hz as a result of sudden phase change of the microgrid voltage during islanding. It then recovers to 60 Hz within approximately one cycle and settles to 59.83 Hz. The last graph of Fig. 17 shows the actual microgrid bus voltages during the islanding transient. It can be seen that the large but short-lived changes in the instantaneous frequency have only minor effect on the phase voltages. These results show that VPD/FQB control scheme is robust to islanding transients even when the VSC output does not match the real and reactive load prior to islanding.

VIII. Conclusion

This paper proposes the VPD/FQB control scheme that allows multiple VSCs with standard inductor interfaces and dq-frame current controls to operate in parallel in a VSC fed microgrid. This control scheme operates in both grid connected and islanded modes and it is independent of the islanding detection circuitry. Moreover, the control scheme provides voltage and frequency regulation of the microgrid in islanded mode, provides inherent over-current protection of the VSC and requires only a single three-phase inductor in the VSC output interface.

In islanded mode, the VPD/FQB controllers set the current references of the VSCs to jointly regulate the voltage and frequency of a common microgrid bus. To make joint voltage control possible, the voltage reference of each VPD/FQB controller is drooped against the d-axis current, and hence the real power output, of the corresponding VSC. Such a droop characteristic also ensures that the VSCs share a common real load in proportion to their voltage droop coefficients. Real power allocation among the VSCs is therefore achieved without control interconnections by drooping the voltage reference. This is in stark contrast to synchronous generators which autonomously share a common load by drooping their frequency references against the mechanical power of the corresponding turbine.

Joint regulation of a common frequency by multiple VSCs and autonomous reactive load sharing is achieved by drooping the frequency reference on each VPD/FQB controller against the q-axis current of the corresponding VSC. This is equivalent to boosting the frequency reference against the reactive power output of the VSC. The use of drooped references also allow VSCs with VPD/FQB controllers to operate in grid connected microgrids since in this case the bus voltage and frequency are dictated by the bulk power system. Moreover, it has been demonstrated that the proposed control scheme is robust to both grid connection and islanding transients.

The motor starting transient of Fig. 12 show that the proposed control scheme has LVRT capability for disturbances originating in the microgrid. In fact, direct online starting of a motor of significant rating (relative to the converter rating) is similar to applying a temporary three phase fault to the microgrid through an impedance. Unlike some distributed resources such as commercial wind farms, a microgrid is designed to island itself to supply high quality power to its critical loads when a low voltage disturbance occurs in the main network [1]. Thus, it will not inject reactive power into the main network to mitigate under-voltage or to help recover from the event.

Acknowledgment

The authors would like to thank D. Fingas for the experimental setup.

References

[1] R. H. Lasseter, "Microgrids," in *Proc. IEEE Power Eng. Soc. Winter Meetting*, Jan. 27–31, 2002, vol. 1, pp. 305–308.

[2] J. Enslin and P. Heskes, "Harmonic interaction between a large number of distributed power inverters and the distribution network," *IEEE Trans. Power Electron.*, vol. 19, no. 6, pp. 1586–1593, Nov. 2004.

[3] I. Erlich and U. Bachmann, "Grid code requirements concerning connection and operation of wind turbines in Germany," in *Proc. IEEE Power Eng. Soc. General Meeting*, Jun. 12–16, 2005, pp. 1253–1257.

[4] J. Holtz, W. Lotzkat, and K. Werner, "A high-power multitransistor-inverter uninterruptable power supply system," *IEEE Trans. Power Electron.*, vol. 3, no. 3, pp. 278–285, Jul. 1988.

[5] T. Kawabata, N. Sashida, Y. Yamamoto, K. Ogasawara, and Y. Yamasaki, "Parallel processing inverter system," *IEEE Trans. Power Electron.*, vol. 6, no. 3, pp. 442–450, Jul. 1991.

[6] A. Martins, A. Carvalho, and A. Araujo, "Design and implementation of a current controller for the parallel operation of standard UPSs," in *Proc. IEEE IECON*, Nov. 6–10, 1995, vol. 1, pp. 584–589.
[7] S. Barsali, M. Ceraolo, P. Pelacchi, and D. Poli, "Control techniques of dispersed generators to improve the continuity of electricity supply," in *Proc. IEEE Power Eng. Soc. Winter Meetting*, Jan. 27–31, 2002, vol. 2, pp. 789–793.
[8] H. Zeineldin, E. El-Saadany, and M. Salama, "Intentional islanding of distributed generation," in *Proc. IEEE Power Eng. Soc. General Meetting*, Jun. 12–16, 2005, pp. 653–659.
[9] P. Piagi and R. H. Lasseter, "Autonomous control of microgrids," in *Proc. IEEE Power Eng. Soc. General Meeting*, Jun. 18–22, 2006.
[10] C. Sao and P. Lehn, "Intentional islanded operation of converter fed microgrids," in *Proc. IEEE Power Eng. Soc. General Meeting*, Jun. 18–22, 2006.
[11] P. Kundur, *Power System Stability and Control*. New York: McGraw-Hill, 1994.
[12] A. Engler and N. Soultanis, "Droop control in lv-grids," in *Proc. 2005 Int. Conf. Future Power Systems*, Nov. 16–18, 2005, vol. 1, pp. 1–6.

Charles K. Sao (M'07) received the B.A.Sc. degree in electrical engineering from the University of British Columbia, Vancouver, BC, Canada, in 2000 and the M.A.Sc and Ph.D. degrees in electrical engineering from the University of Toronto, Toronto, ON, Canada, in 2002 and 2007.

From January to December 2000, he was with British Columbia Hydro and Power Authority in Vancouver. Currently, he works for Kestrel Power Engineering Ltd. in Toronto.

Peter W. Lehn (SM'05) received the B.Sc. and M.Sc. degrees in electrical engineering from University of Manitoba, Winnipeg, MB, Canada, in 1990 and 1992, respectively, and the Ph.D. degree in electrical engineering from the University of Toronto, Toronto, ON, Canada, in 1999.

From 1992 to 1994, he was with the Network Planning Group of Siemens AG, Erlangen, Germany. Currently, he is an Associate Professor at the University of Toronto.